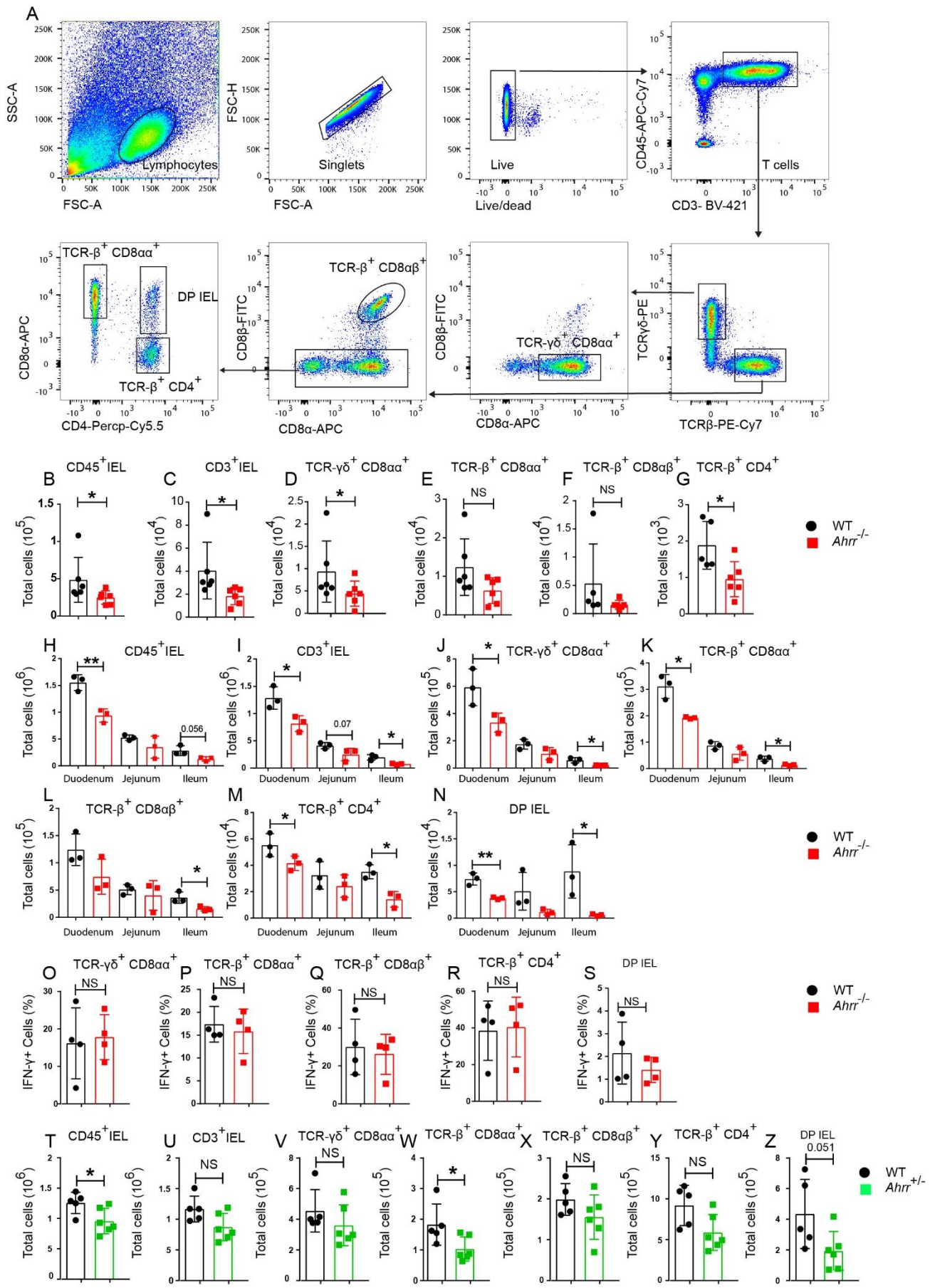
A
SSC-A
FSC-A
Lymphocytes
FSC-H
FSC-A
Singlets
Live
Live/dead
CD45-APC-Cy7
CD3- BV-421
T cells
TCR-β+ CD8αα+
DP IEL
TCR-β+ CD4+
CD8α-APC
CD4-Percp-Cy5.5
TCR-β+ CD8αβ+
CD8β-FITC
CD8α-APC
TCR-γδ+ CD8αα+
CD8β-FITC
CD8α-APC
TCRγδ-PE
TCRβ-PE-Cy7
B CD45+IEL
C CD3+IEL
D TCR-γδ+ CD8αα+
E TCR-β+ CD8αα+
F TCR-β+ CD8αβ+
G TCR-β+ CD4+
Total cells (10^5)
Total cells (10^4)
Total cells (10^3)
NS
WT
Ahrr-/-
H CD45+IEL
I CD3+IEL
J TCR-γδ+ CD8αα+
K TCR-β+ CD8αα+
Total cells (10^6)
Total cells (10^5)
0.056
0.07
Duodenum
Jejunum
Ileum
L TCR-β+ CD8αβ+
M TCR-β+ CD4+
N DP IEL
O TCR-γδ+ CD8αα+
P TCR-β+ CD8αα+
Q TCR-β+ CD8αβ+
R TCR-β+ CD4+
S DP IEL
IFN-γ+ Cells (%)
T CD45+IEL
U CD3+IEL
V TCR-γδ+ CD8αα+
W TCR-β+ CD8αα+
X TCR-β+ CD8αβ+
Y TCR-β+ CD4+
Z DP IEL
0.051
WT
Ahrr+/-

Figure S1. *Ahrr*$^{-/-}$ mice have reduced numbers of colonic IEL, related to Figure 1. **(A)** Gating strategy for IEL-Lymphocyte sized live cells were gated for CD3 and CD45. CD45^{+}, CD3^{+} cells were further analyzed for expression of TCRγδ and TCRαβ. TCRγδ^{+} and TCRαβ^{+} cells were classified into different subsets of IEL based on expression of CD4, CD8α and CD8β as indicated. **(B**) Numbers of CD45^{+} IEL in the large intestine of WT and *Ahrr*$^{-/-}$ mice. **(C)** Numbers of T cells in the epithelium of the large intestine. **(D-F)** IEL populations in large intestine epithelium of WT and *Ahrr*$^{-/-}$ mice, including TCR-γδ^{+} CD8αα^{+} **(D)**, TCR-β^{+} CD8αα^{+} **(E)**, TCR-β^{+} CD8αβ^{+} **(F)**, and TCR-β^{+} CD4^{+} **(G)**. **(H-N)** IEL populations in proximal, intermediate and distal segments of the small intestine of WT and *Ahrr*$^{-/-}$ mice, including CD45^{+} **(H)**, CD3^{+} **(I),** TCR-γδ^{+} CD8αα^{+} **(J)**, TCR-β^{+} CD8αα^{+} **(K)**, TCR-β^{+} CD8αβ^{+} **(L)**, TCR-β^{+} CD4^{+} **(M)** and DP IEL **(N)**. **(O-S)** Percentage of IFN-γ^{+} IEL in WT and *Ahrr*$^{-/-}$ mice. **(T-Z)** IEL populations in the small intestine of WT and *Ahrr*$^{+/-}$ mice, including CD45^{+} **(T)**, CD3^{+} **(U),** TCR-γδ^{+} CD8αα^{+} **(V)**, TCR-β^{+} CD8αα^{+} **(W)**, TCR-β^{+} CD8αβ^{+} **(X)**, TCR-β^{+} CD4^{+} **(Y)** and DP IEL **(Z)**. Each dot represents an individual mouse. Data are representative of 2-3 individual experiments. Statistical significance was determined by Mann-Whitney test. *P<0.05.

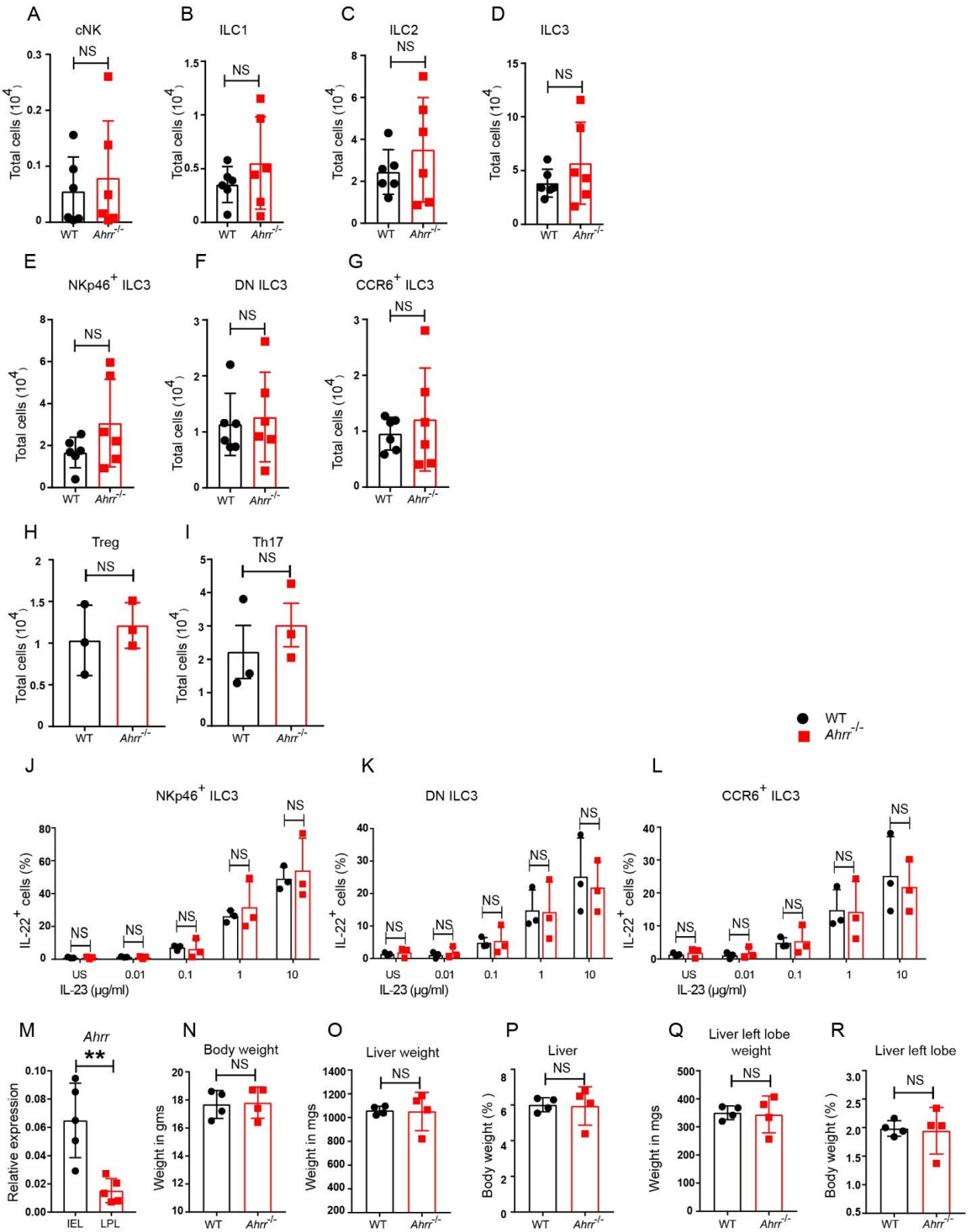
A
cNK
NS
Total cells (10^4)
WT
Ahrr-/-
B
ILC1
C
ILC2
D
ILC3
E
NKp46+ ILC3
F
DN ILC3
G
CCR6+ ILC3
H
Treg
I
Th17
WT
Ahrr-/-
J
NKp46+ ILC3
K
DN ILC3
L
CCR6+ ILC3
IL-22+ cells (%)
US
0.01
0.1
1
10
IL-23 (µg/ml)
M
Ahrr
**
Relative expression
IEL
LPL
N
Body weight
Weight in gms
O
Liver weight
Weight in mgs
P
Liver
Body weight (%)
Q
Liver left lobe weight
R
Liver left lobe

Figure S2. ILC and liver are unaffected by *Ahrr* deficiency, related to Figure 1. (A-I) Absolute numbers of different cell populations in lamina propria of WT and *Ahrr*$^{-/-}$ mice: conventional NK cells (cNK) **(A)**, ILC1 **(B)**, ILC2 **(C)**, ILC3 **(D)**, NKp46^{+} ILC3 **(E)**, NKp46^{-} CCR6^{-} **(F)**, CCR6^{+} ILC3 **(G)**, Treg **(H)**, and Th17 **(I)** in the lamina propria of WT and *Ahrr*$^{-/-}$ mice remain comparable (gating strategy described in the method section). **(J-L)** IL-22 production by different subsets of ILC3 in response to IL-23 in-vitro. **(M)** Expression of *Ahrr* mRNA in IEL (CD8^{+}) vs lamina propria T cells (CD8^{+}). **(N-R)** analysis of livers of age- and sex-matched 8-10 weeks old WT and *Ahrr*$^{-/-}$ mice: body weight **(N)**, liver weight **(O)**, liver weight as percentage of body weight **(P)**, liver left lobe weight **(Q)** and liver left lobe weight as percentage of body weight **(R)**. Each dot represents an individual mouse. Data are representative of 2-3 individual experiments. Statistical significance was determined by Mann-Whitney test. *P<0.05, **P<0.01, ***P<0.001.

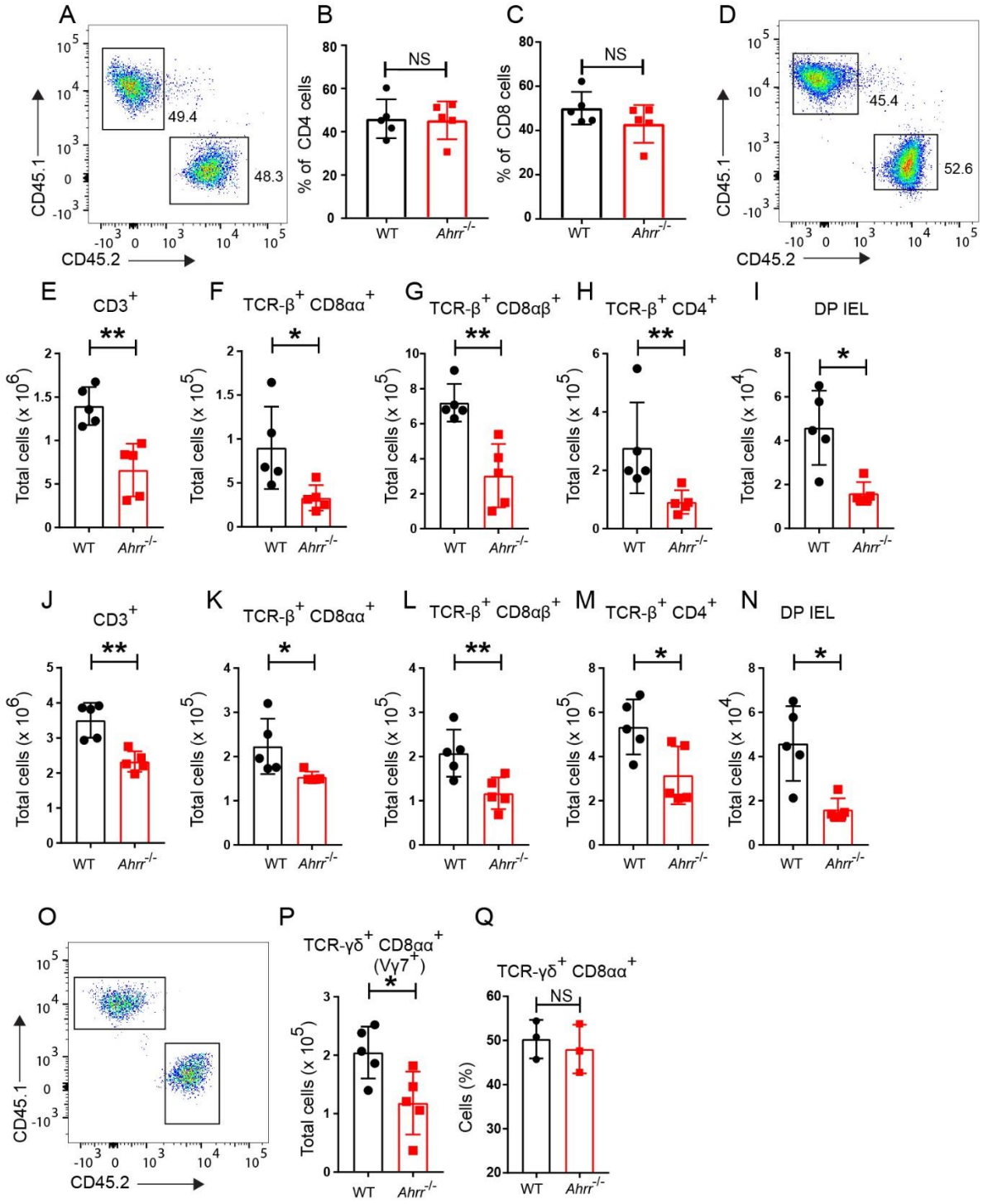
A
B
C
D
CD45.1
CD45.2
49.4
48.3
45.4
52.6
% of CD4 cells
% of CD8 cells
NS
WT
Ahrr-/-
E
F
G
H
I
CD3+
TCR-β+ CD8αα+
TCR-β+ CD8αβ+
TCR-β+ CD4+
DP IEL
Total cells (x 10^6)
Total cells (x 10^5)
Total cells (x 10^4)
**
*
J
K
L
M
N
O
P
Q
TCR-γδ+ CD8αα+ (Vγ7+)
Cells (%)

Figure S3. Reconstitution of splenic T cells in mixed bone marrow chimeric mice, related to Figure 2. Splenic T cells of chimeric mice reconstituted with bone marrow cells from WT (CD45.1) and *Ahrr*$^{-/-}$ (CD45.2) mice in 1:1 ratio. **(A)** Representative FACS plot showing splenic CD4^{+} T cells. **(B,C)** Frequency of WT and *Ahrr*$^{-/-}$ splenic CD4 and CD8 T cells. **(D)** Representative FACS plot showing frequency of WT CD45.1 and *Ahrr*$^{+/+}$ CD45.2 CD4 IEL recovered from small intestine after adoptive transfer. **(E-I)** Numbers of small intestinal WT and *Ahrr*$^{-/-}$ CD3^{+} IEL **(E)**, TCR-β^{+} CD8αα^{+} IEL **(F)**, TCR-β^{+} CD8αβ^{+} IEL **(G)**; TCR-β^{+} CD4^{+} IEL **(H)** and DP-IEL **(I)** recovered after adoptive transfer. **(J-N)** Numbers of small intestinal WT and *Ahrr*$^{-/-}$ CD3^{+} IEL **(J)**, TCR-β^{+} CD8αα^{+} IEL **(K)**, TCR-β^{+} CD8αβ^{+} IEL **(L)**; TCR-β^{+} CD4^{+} IEL **(M)**; DP-IEL **(N)** recovered after bone marrow chimera**. (O)** FACS plot depicting frequency of WT CD45.1 and *Ahrr*$^{+/+}$ CD45.2 CD4 IEL recovered from small intestine after mix bone marrow chimera. **(P) Numbers of** TCR-γδ^{+} CD8αα^{+} (vγ7) IEL and **(Q)** Frequency of small intestinal WT and *Ahrr*$^{-/-}$ TCR-γδ^{+} CD8αα^{+} IEL recovered after bone marrow chimera**.** Each dot represents an individual mouse. Statistical significance was determined by Mann-Whitney test. *P<0.05, **P<0.01.

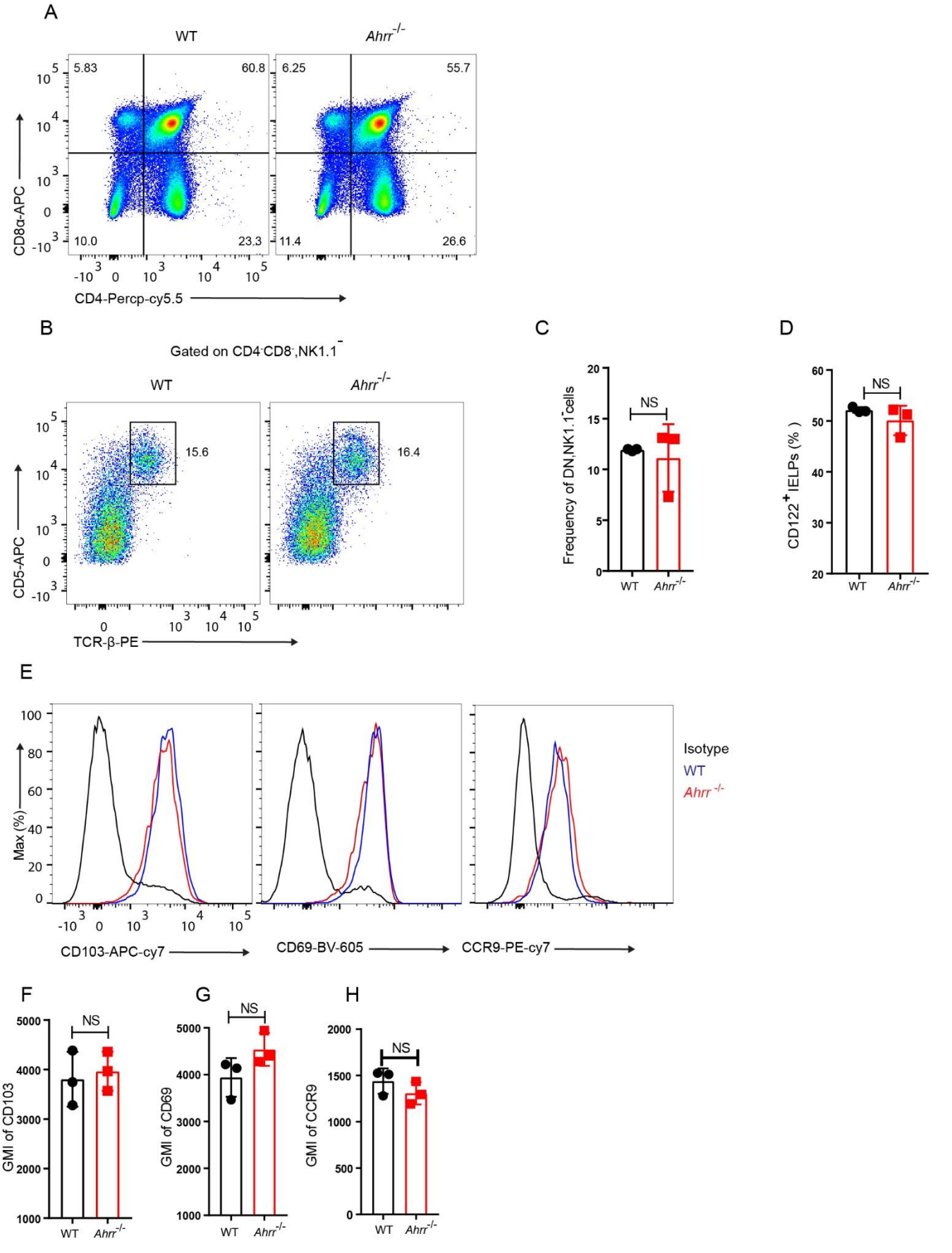
A
WT
Ahrr-/-
5.83
60.8
10.0
23.3
6.25
55.7
11.4
26.6
CD8α-APC
CD4-Percp-cy5.5
B
Gated on CD4-CD8-,NK1.1-
WT
Ahrr-/-
15.6
16.4
CD5-APC
TCR-β-PE
C
Frequency of DN,NK1.1-cells
NS
WT
Ahrr-/-
D
CD122+IELPs (%)
NS
WT
Ahrr-/-
E
Max (%)
Isotype
WT
Ahrr -/-
CD103-APC-cy7
CD69-BV-605
CCR9-PE-cy7
F
GMI of CD103
NS
WT
Ahrr-/-
G
GMI of CD69
NS
WT
Ahrr-/-
H
GMI of CCR9
NS
WT
Ahrr-/-

Figure S4. IEL development and homing are independent of AHRR, related to Figures 1 and 2. (A) FACS analysis of different CD4 and CD8 cell populations in thymus of WT and *Ahrr*$^{-/-}$ mice. **(B)** Representative FACS plots showing frequency of IELp in WT and *Ahrr*$^{-/-}$ mice. **(C,D)** Frequency of IELp and CD122^{+}IELp in WT and *Ahrr*$^{-/-}$ mice. **(E-H)** Representative histograms **(E)** and GMI **(F,H)** of CD103, CD69 and CCR9 expression on DP IEL of WT and *Ahrr*$^{-/-}$ mice. Each dot represents an individual mouse. Data are representative of 2-3 individual experiments. Statistical significance was determined by Mann-Whitney test.

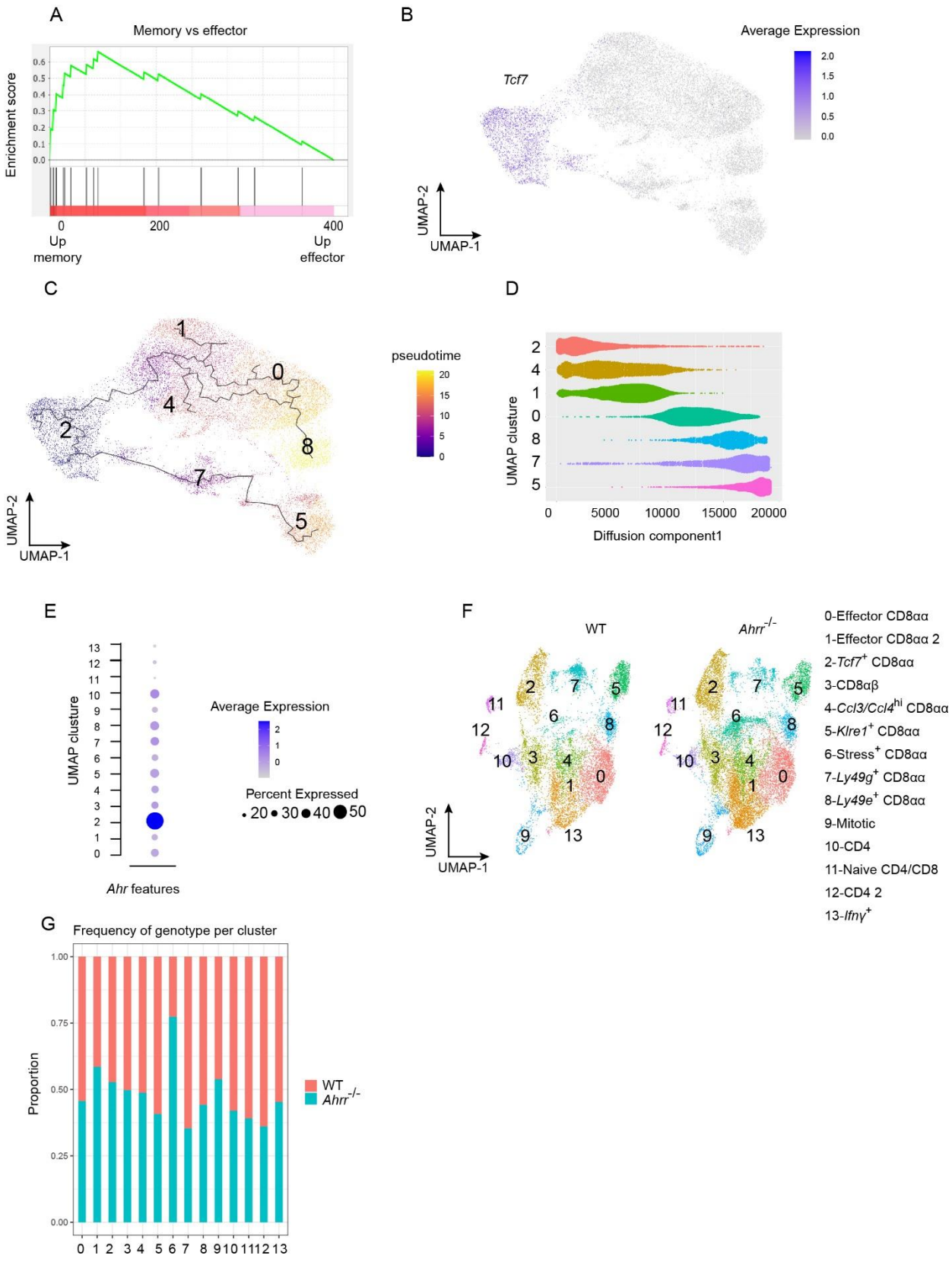
A
Memory vs effector
Enrichment score
0.6
0.5
0.4
0.3
0.2
0.1
0.0
0
200
400
Up
memory
Up
effector
B
Average Expression
Tcf7
2.0
1.5
1.0
0.5
0.0
UMAP-2
UMAP-1
C
1
0
4
2
8
7
5
UMAP-2
UMAP-1
pseudotime
20
15
10
5
0
D
UMAP cluster
2
4
1
0
8
7
5
0
5000
10000
15000
20000
Diffusion component1
E
UMAP cluster
13
12
11
10
9
8
7
6
5
4
3
2
1
0
Ahr features
Average Expression
2
1
0
Percent Expressed
20
30
40
50
F
WT
Ahrr-/-
2
7
5
11
6
8
12
10
3
4
1
0
9
13
UMAP-2
UMAP-1
0-Effector CD8αα
1-Effector CD8αα 2
2-Tcf7+ CD8αα
3-CD8αβ
4-Ccl3/Ccl4hi CD8αα
5-Klre1+ CD8αα
6-Stress+ CD8αα
7-Ly49g+ CD8αα
8-Ly49e+ CD8αα
9-Mitotic
10-CD4
11-Naive CD4/CD8
12-CD4 2
13-Ifnγ+
G
Frequency of genotype per cluster
Proportion
1.00
0.75
0.50
0.25
0.00
0 1 2 3 4 5 6 7 8 9 10 11 12 13
WT
Ahrr-/-

Figure S5. A subset of IEL display memory precursor like phenotype, related to Figure 3. (A) Gene set enrichment analysis for *Tcf7*$^{+}$ CD8αα^{+} cells (cluster 2 described in **Figure 3A**)**. (B,C)** UMAP and pseudo time trajectory analysis of *Tcf7* expression in IEL clusters. **(D)** IEL clusters ordered along diffusion component. **(E)** Comparative analysis of *Ahr* features in different IEL clusters. **(F,G)** UMAP plot and frequency of various populations of IEL from WT and *Ahrr*$^{-/-}$ mice.

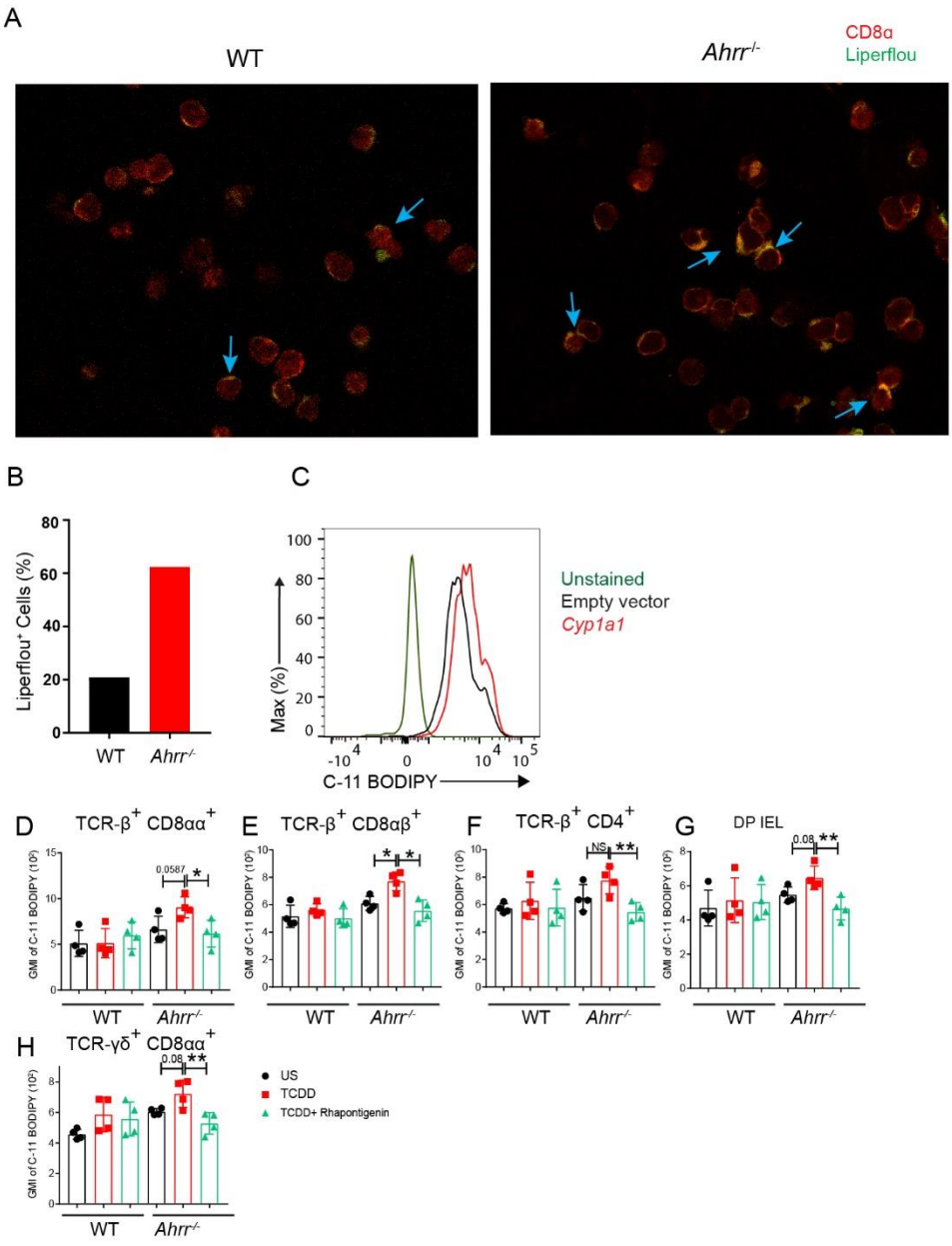

Figure S6. AHRR deficiency induce ferroptosis in IEL, related to Figure. 4. IEL from WT and *Ahrr*$^{-/-}$ mice were stained for CD8α and Liperflou. **(A)** Image showing Liperflou (green) staining of CD8α+ cells (red). **(B)** % of Liperflou^{+} cells. **(C)** Histograms depicting C-11 BODIPY staining of Jurkat cells transduced with *Cyp1a1* or vector only and unstained cells. The results are representative of two independent experiments. **(D-H)** C-11 BODIPY staining of WT and *Ahrr*$^{-/-}$ IEL upon TCDD stimulation with and without

Rhapontigenin in different IEL subsets. Each dot represents a mouse. Statistical significance was determined by Mann-Whitney test. *P<0.05, **P<0.01, **P<0.001.

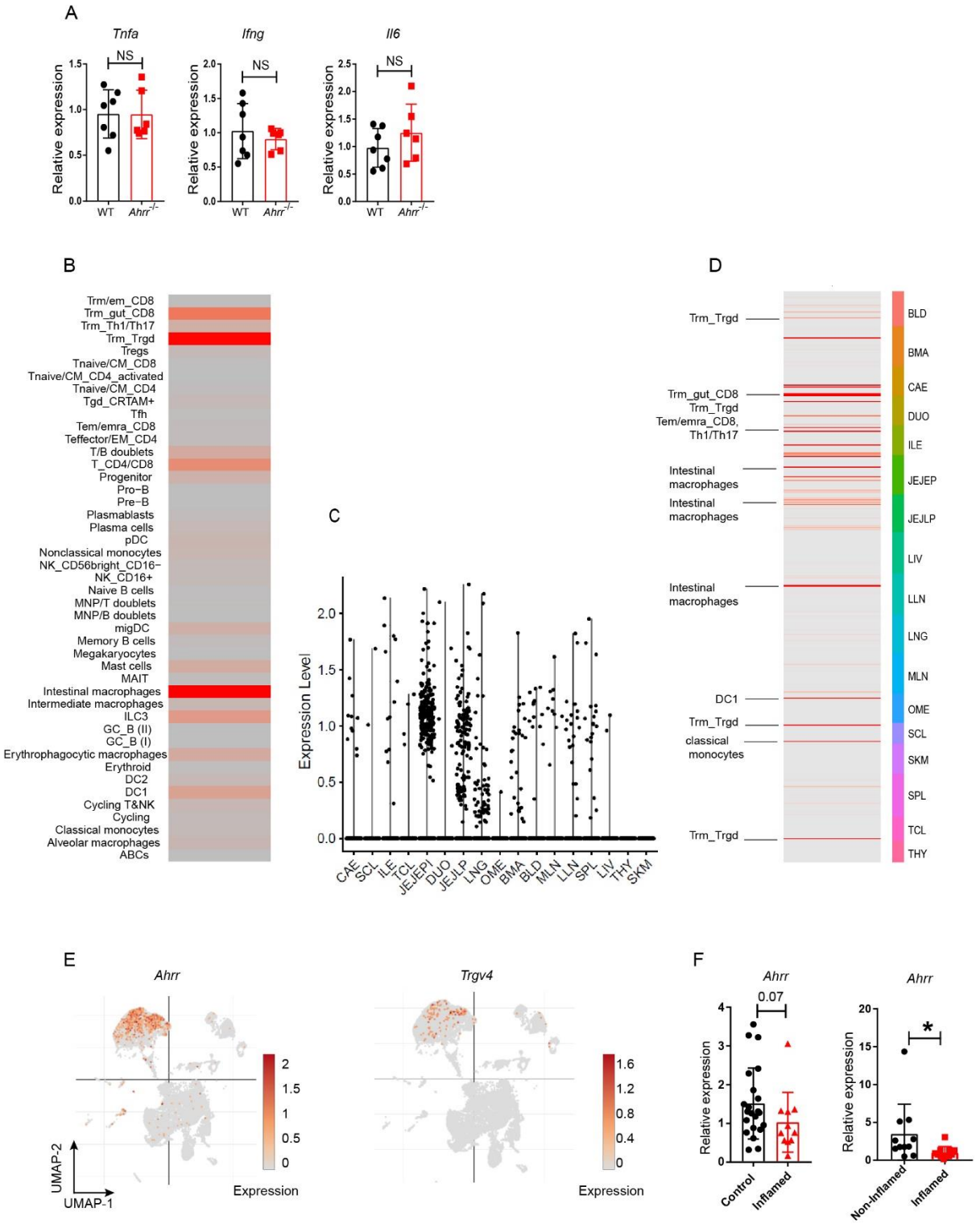

Figure S7. AHRR impact and expression in mouse and human intestinal pathology, related to Figure 7. (A) Spontaneous tissue inflammation is not induced in *Ahrr*$^{-/-}$ mice. Ileal tissues of WT and *Ahrr*$^{-/-}$ mice were analyzed for RNA levels of *Tnfa*, *Il6* and *Ifng*. Each dot represents an individual mouse. Data are from 2 individual experiments pooled. **(B)** Average *Ahrr* expression across all manually curated human cell types in the Cross-Tissue Immune Cell Atlas (CTICA). **(C)** Violin plot representing the scaled expression of *AHRR* across each human organ (all cell types combined); each dot represents a cell. **(D)** Average *Ahrr* expression across different cell types and across the human organs sequenced in the creation of the CTICA. Annotated are cell types in tissues that have very high expression. **(E)** Single cell analysis of digestive system enteropathies reveals a cluster of cells that expresses *Ahrr* and *Trgv4*, corresponding to *Ahrr*$^{+}$ intestinal γδ T cells; UMAP plots were extracted from the Broad Single Cell portal. **(F)** *Ahrr* expression in control (healthy), non-inflamed and inflamed tissues of IBD patients. Statistical significance was determined by Mann-Whitney test. *P<0.05.